QUANTUM GASES

Evidence of superfluidity in a dipolar supersolid from nonclassical rotational inertia

L. Tanzi[1,2], J. G. Maloberti[1,2], G. Biagioni[1,2], A. Fioretti[1], C. Gabbanini[1], G. Modugno[1,2]*

A key manifestation of superfluidity in liquids and gases is a reduction of the moment of inertia under slow rotations. Nonclassical rotational effects have also been considered in the context of the elusive supersolid phase of matter, in which superfluidity coexists with a lattice structure. Here, we show that the recently discovered supersolid phase in dipolar quantum gases features a reduced moment of inertia. Using a dipolar gas of dysprosium atoms, we studied a peculiar rotational oscillation mode in a harmonic potential, the scissors mode, previously investigated in ordinary superfluids. From the measured moment of inertia, we deduced a superfluid fraction that is different from zero and of order of unity, providing direct evidence of the superfluid nature of the dipolar supersolid.

Superfluids exhibit their most spectacular properties during rotation. This is because the superfluid state is described by a macroscopic wave function, the phase of which can change only by integer multiples of 2π upon completing a closed path. For a cylindrical superfluid rotating at low angular velocities, $\omega \to 0$, this condition leads to the vanishing of both angular momentum L and moment of inertia $I = \langle L \rangle / \omega$. An angular momentum can appear only for sufficiently large ω at integer multiples of the reduced Planck's constant $\hbar$, through the appearance of quantized vortices. These nonclassical rotational effects have been verified for most known superfluids: nuclear matter (*1*), ^{4}He (*2*), ^{3}He (*3*), gaseous Bose-Einstein condensates (*4*), degenerate Fermi gases (*5*), and exciton-polariton condensates (*6*). A related phenomenon is the Meissner effect in superconductors (*7*).

At the end of the 1960's, another type of bosonic phase of matter described by a macroscopic wave function, the supersolid, was predicted to exist. In a supersolid, superfluidity coexists with a crystal-type structure (*8*–*10*). A. J. Leggett suggested that a rotating supersolid should show a moment of inertia intermediate between that of a superfluid and that of a classical system, $I = (1 - f_s)\, I_c$. Here, I_c is the classical moment of inertia and $0 \le f_s \le 1$ is the so-called superfluid fraction (*10*). This phenomenon is called nonclassical rotational inertia (NCRI). Standard superfluids can have $f_s < 1$, but only at finite temperature, $T > 0$, because of the presence of a thermal component. In a supersolid at $T = 0$, the reduction of the superfluid fraction is instead caused by the spatially modulated density, which tends to increase the inertia toward the classical limit (*10*, *11*).

At the time it was proposed, the primary candidate for observing supersolidity was solid helium. Torsion oscillators were used extensively to attempt detecting NCRI (*12*). The original announcement of the possible presence of a large superfluid fraction, $f_s \approx 10^{-1}$ (*13*, *14*), later received a different interpretation based on a change of the elastic properties of the solid (*15*) and has not been confirmed by more recent studies (*16*). Superfluidity in bulk solid helium has now been excluded down to the level of 10^{-4} (*17*), and the search goes on in two-dimensional (2D) films (*18*).

We studied a different supersolid candidate, a gaseous Bose-Einstein condensate (BEC) of strongly dipolar atoms in which a density-modulated regime coexisting with the phase coherence necessary for supersolidity has been recently discovered (*19*–*21*). So far, its superfluid nature has been tested through nonrotational excitation modes that can be described in terms of the hydrodynamic equations for superfluids (*22*–*24*). Here, we aimed instead at characterizing the NCRI of such a system, searching for direct evidence of superfluidity under rotation, in the spirit of the helium experiments.

Achieving dipolar supersolids large enough to realize a cylindrical geometry has so far not been possible, so we used a specific rotation technique that fits the asymmetric, small-sized systems available in the laboratory. We excited the so-called scissors mode, a small-angle rotational oscillation of the harmonic potential that naturally holds the system. This technique, inspired by an excitation mode of nuclei (*25*), has been proposed (*26*, *27*) and used (*28*) to demonstrate the superfluidity of ordinary BECs. A recent theoretical study has shown that the scissors mode can also be used to characterize the NCRI of a dipolar supersolid (*29*). We studied the change of the scissors mode frequency across the transition from BEC to the supersolid regime to directly compare the supersolid with a fully superfluid system.

In this experiment, a BEC of strongly magnetic Dy atoms is held in an anisotropic harmonic trap, with frequencies $\omega_{x,y,z} = 2\pi\,(23,46,90)\ \mathrm{s}^{-1}$, with the dipoles oriented in the z direction by a magnetic field B (Fig. 1). The temperature is sufficiently low to have a negligible thermal component (*30*). We induced the transition from BEC to supersolid by tuning through a magnetic Feshbach resonance the interaction parameter ε_{dd}, which parametrizes the ratio of the dipolar and van der Waals interaction energies (*19*). In the supersolid regime, a density modulation develops along the weak x axis, leading to the appearance of interference peaks in the momentum distribution. We know our lattice to be composed of two principal density maxima, or "droplets," each containing ~10^4 atoms (*22*). This realizes a so-called cluster supersolid (*31*), very different from the hypothesized helium supersolid with one particle per lattice site. In principle, further tuning of ε_{dd} would bring the system into the so-called droplet crystal regime, with no coherence between the droplets (*19*–*21*).

The scissors mode is excited by changing suddenly the direction of the eigenaxes of the harmonic trap (*30*). This results in a sinusoidal oscillation with frequency ω_{sc} of the angle θ between the long axis of the system and the corresponding trap axis. We chose to rotate the system in the (x,y) plane, perpendicular to the direction of the dipoles, so that the dipolar interaction potential would be independent of θ (*32*, *33*).

The oscillation frequency can be directly related to the moment of inertia of the superfluid through the following equation:

$$I = I_c\, \alpha\, \beta\, (\omega_x^2 + \omega_y^2)/\omega_{sc}^2 \qquad (1)$$

Where $\alpha = (\omega_y^2 - \omega_x^2)/(\omega_y^2 + \omega_x^2)$ and $\beta = \langle x^2 - y^2 \rangle / \langle x^2 + y^2 \rangle$ are geometrical factors measuring the deviation from cylindrical symmetry of the trap and of the density distribution, respectively (*26*, *29*). Whereas α can be measured experimentally, β needs to be calculated theoretically (*30*). For nondipolar BECs in the Thomas-Fermi regime, one has the simplification $\beta = \alpha$ (*27*). For dipolar systems, the density deformation changes instead with the interaction parameter because of magnetostriction, $\beta = \beta(\varepsilon_{dd}) \neq \alpha$ (*32*). If the oscillation amplitude is much smaller than β, then the density deformation stays constant during the motion (*26*).

We can now connect the moment of inertia to a superfluid fraction, which we define specifically for our system in analogy with Leggett's definition, taking into account our noncylindrical geometry as follows:

$$I = (1 - f_s)\, I_c + f_s\, \beta^2\, I_c \qquad (2)$$

It is easy to see that this definition coincides with Leggett's one in the cylindrical case, $\beta = 0$. It also coincides with the known results

[1]CNR-INO, Sede Secondaria di Pisa, 56124 Pisa, Italy. [2]LENS and Dipartimento di Fisica e Astronomia, Università di Firenze, 50019 Sesto Fiorentino, Italy.
*Corresponding author. Email: modugno@lens.unifi.it

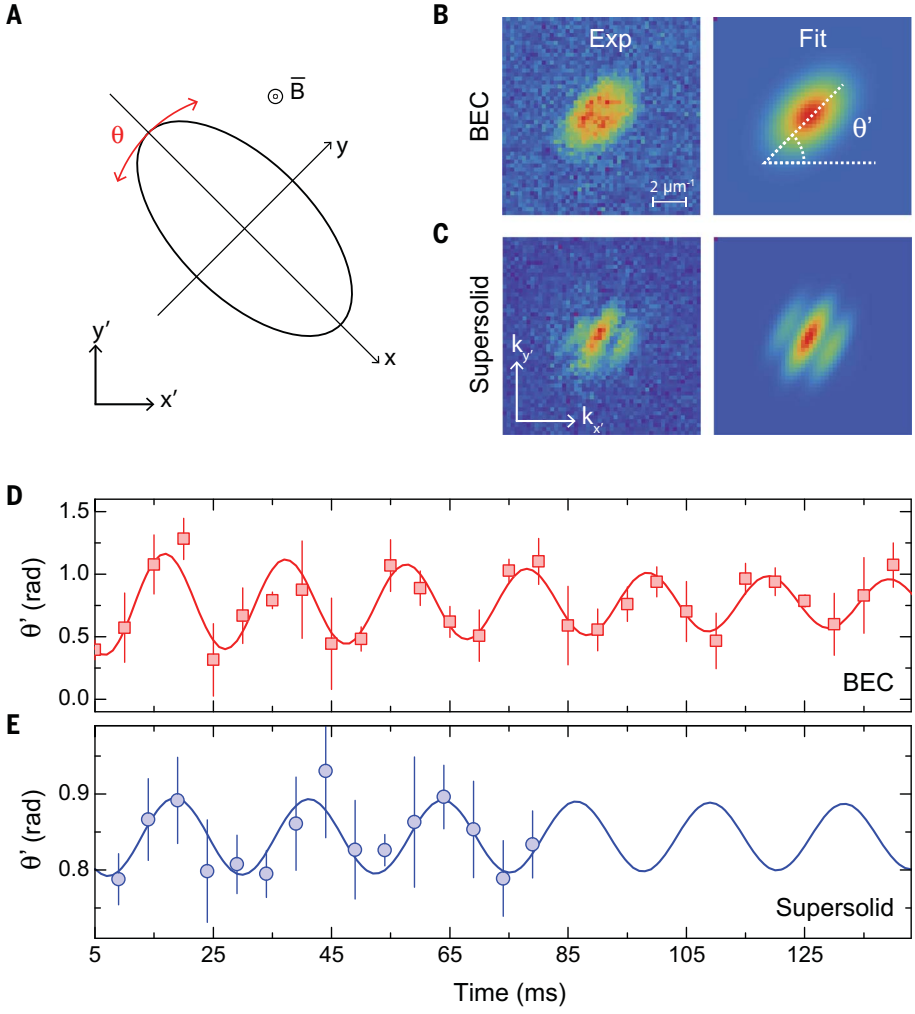

Fig. 1. Scissors mode measurements. (**A**) Sketch of the experimental geometry. The atomic system (ellipse) is trapped in an anisotropic potential with eigenaxes *x* and *y*. A sudden rotation of the trapping potential excites an angular oscillation θ(*t*) (red arrows). (**B** and **C**) Examples of the experimental distributions after free expansion and of the corresponding 2D fits used for extracting the oscillation angle θ′ after the free expansion in the BEC regime [ε_{dd} = 1.14 (B)] and the supersolid regime [ε_{dd} =1.45 (C)]. (**D** and **E**) Time evolution of the angle θ′(*t*) in the BEC regime (D) and the supersolid regime (E). Error bars represent the SD of four to eight measurements.

for a superfluid with elliptical geometry, $I = \beta^2 I_c$ (*1*, *26*, *34*). The presence of a residual moment of inertia in the BEC, despite $f_s = 1$ at $T = 0$, derives from a peculiar velocity distribution, which is very different from the one in a cylindrical geometry (*26, 27*). Finally, by combining Eqs. 1 and 2, one can directly relate the superfluid fraction to the trap and scissors frequencies and to the deformation as follows:

$$f_s = [1 - \alpha\beta(\omega_x^2 + \omega_y^2)/\omega_{sc}^2]/(1 - \beta^2) \quad (3)$$

We note that the scissors mode is analogous to the helium torsion oscillators because both detect NCRI through the oscillation frequency (*13*–*16*), although there are some differences. In the scissors mode, all atoms experience the restoring force from the trap, so there are no elastic effects to consider (*15*). A finite deformation β is clearly necessary for the scissors mode, whereas torsion oscillators are normally symmetric, although macroscopic deformations can be taken into account with the same formalism (*34, 35*) and a related tortuosity effect is present for superfluids in porous media (*13*).

Let us now turn to the experimental results. Figure 1, B to E, summarizes the scissors measurements in the BEC and supersolid regimes. The 2D density distributions are imaged after a free expansion of the system, representing effective momentum distributions. They are fitted to extract the angle θ′ in the laboratory frame for various observation times *t*. The resulting data for θ′(*t*) are fitted with a sinusoid to measure ω_{sc} (*30*). Both the BEC and supersolid regimes feature single-frequency oscillations, as expected for weakly interacting superfluids (*26*). We ensured that a thermal sample featured instead a two-frequency oscillation, as expected for a weakly interacting system [fig. S1 (*30*)].

To avoid perturbations caused by other collective modes (*30*), we used two different excitation techniques for the BEC and the supersolid regimes, which result in a lower amplitude of the scissors mode for the supersolid (Fig. 1, D and E). The accuracy in the determination of the scissors frequency in that regime is limited also by the finite lifetime of the supersolid (*19*).

A summary of the experimental results for the scissors frequency and the related moment of inertia is shown in Fig. 2. The results are compared with the theoretical predictions of (*29*), calculated for trap parameters and atom numbers close to the experimental ones. For the BEC, we measure a frequency that depends only weakly on the interaction parameter ε_{dd}, consistent with the prediction of a weak change of the deformation β (ε_{dd}) (*32*). By contrast, when the system enters the supersolid regime, we observed a clear reduction of the frequency, in agreement with the theory. From the measured frequency, we can determine the moment of inertia I/I_c through Eq. 1, where the deformation β is determined from the numerically calculated density distributions (*29*). These results are shown in Fig. 2B. In the BEC regime, the moment of inertia differs by a factor of two from the classical value and the ratio I/I_c is consistent with β^2, as expected for a fully superfluid system. In the supersolid regime, at ε_{dd} = 1.45, the moment of inertia increases toward the classical value but does not reach it. This provides evidence of NCRI for the dipolar supersolid.

The data point in Fig. 2B further in the supersolid regime, at ε_{dd} = 1.5, has larger error bars because of the shorter lifetime of the system. We were unable to study the droplet crystal regime, which is predicted to appear for $\varepsilon_{dd} \approx 1.52$ (*29*) because of the loss of the interference pattern (*19*–*21*).

The change of I/I_c is in principle caused by both the change of shape, β (ε_{dd}), when the supersolid modulation forms and the related change of the superfluid fraction. The experiment-theory agreement for I/I_c both in the BEC regime, where $f_s = 1$, and at ε_{dd} =1.45, where *I* is expected to be close to I_c, supports the validity of the calculated β for our system. Equation 2 shows that if the superfluid fraction of the supersolid varies between 0 and 1, then I/I_c shown in Fig. 2B should vary between 1 and β^2. More directly, we calculate the superfluid fraction from Eq. 3, using the experimental frequencies and the theoretical β. The results are shown in Fig. 3, together with

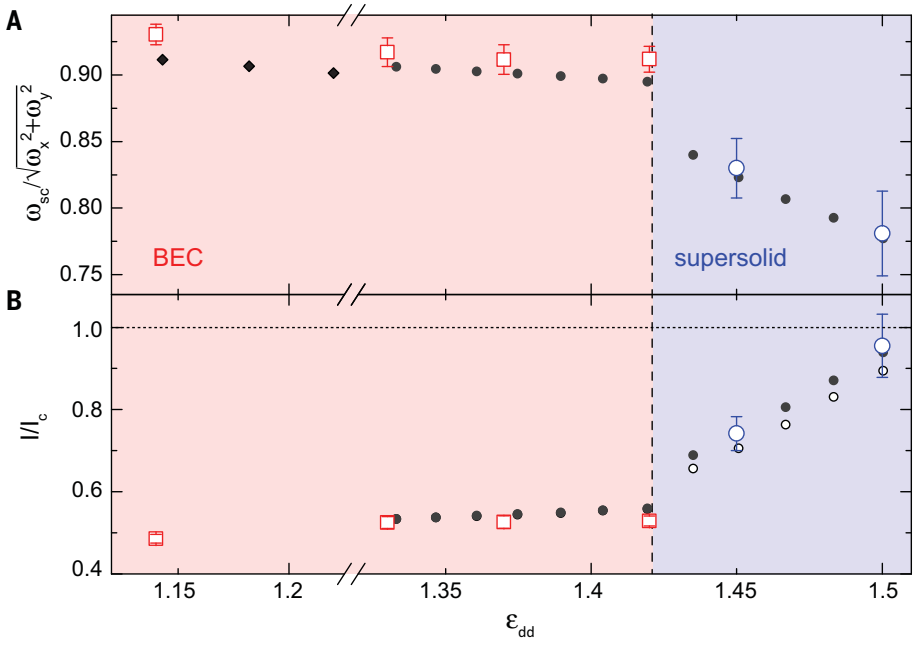

Fig. 2. Scissors mode frequency and moment of inertia versus the interaction parameter. (**A**) Scissors mode frequencies. Large circles and squares are the experimental measurements. Black diamonds and dots are the mean-field and beyond-mean-field theoretical predictions, respectively (*29, 32*). (**B**) Moment of inertia. Large squares and circles are derived from Eq. 1 using the experimental measurements of the scissors frequencies and the theoretical β (*29*). Black dots are the numerical simulation (*29*). Small open dots are the theoretical prediction for β^2 (*29*). Error bars indicate 1 SD (*30*). In the experiment, ε_{dd} has a calibration uncertainty of 3%. The dashed line separating the BEC and supersolid regimes was determined numerically (*29*).

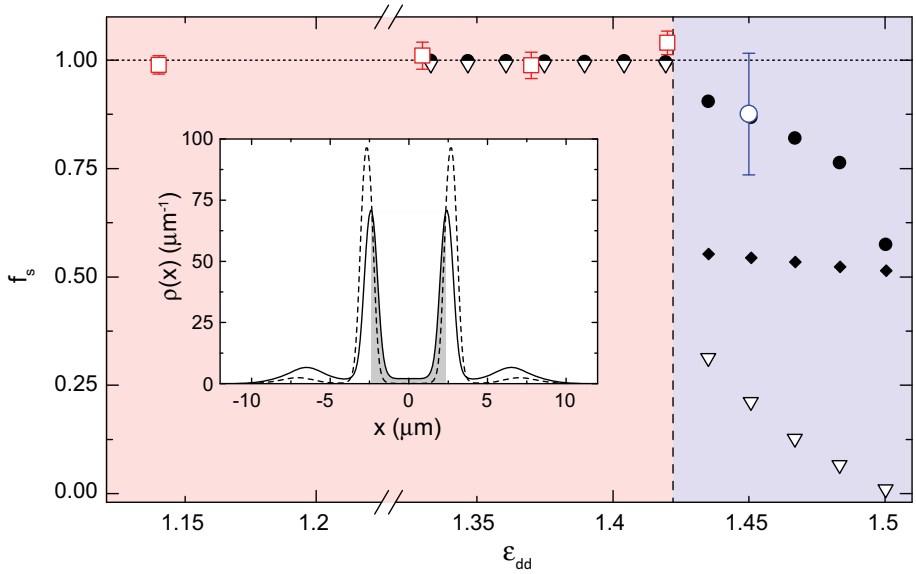

Fig. 3. Superfluid fraction from BEC to supersolid. Red squares and blue circle are the superfluid fraction from the experimentally measured scissors frequency and the theoretical β using Eq. 3, respectively. Black dots are the superfluid fraction from the theoretical frequency (*29*). Open triangles are the upper limit for the 1D superfluid fraction from Eq. 4. Diamonds are the estimated superfluid fraction of independent droplets. Inset shows the calculated mean density distribution (30) for ε_{dd} = 1.45 (continuous line) and ε_{dd} = 1. 5 (dashed line). Gray indicates the region of integration for Eq. 4.

the corresponding points calculated from the theoretical predictions of (*29*).

In the BEC regime, the data confirm that the system is fully superfluid, $f_s = 1$, as already found for nondipolar BECs (*28*). In the supersolid regime, we can reliably calculate the superfluid fraction only for the experimental data point at $\varepsilon_{dd} = 1.45$. Unexpectedly, the superfluid fraction of the supersolid is very large, $f_s \approx 0.9$, in agreement with the numerical calculations. Given the measurement uncertainty, f_s is consistent with unity and inconsistent with zero. This result demonstrates the superfluid nature of the dipolar supersolid under rotation.

The theory predicts a reduction of the superfluid fraction moving further into the supersolid regime, although f_s remains finite even in the droplet crystal regime because of the superfluidity of the individual droplets under rotation (*29*). In the experiment, we cannot check whether f_s decreases moving to $\varepsilon_{dd} = 1.5$ because the lower measurement accuracy and the increase of β^2 shown in Fig. 2B prevent us from measuring f_s reliably (*30*).

It is interesting to compare our results with the original prediction by Leggett for the superfluid fraction of a supersolid rotating in a 1D annulus,

$$f_s \leq [\int dx/\rho(x)]^{-1} \qquad (4)$$

where $\rho(x)$ is the normalized density along the annulus and the integral is performed on a lattice cell (*10*, *11*). Equation 4 shows that the reduction of the superfluid fraction is a consequence of the breaking of translational invariance, because f_s is determined by the minimum density between lattice sites. Intuitively, in a homogeneous superfluid, $\rho(x)$ = constant implies that each atom is equally delocalized so no rotation happens. In a system where $\rho(x) \to 0$ between neighboring lattice sites, the sites are distinguishable, so the system rotates classically. The supersolid is the intermediate case in which the atoms are still delocalized, but the density modulation allows a partial rotation, increasing the moment of inertia compared with a homogeneous superfluid.

In 1970, Leggett used Eq. 4 and the known information on the helium lattice to estimate $f_s < 10^{-4}$ for solid helium (*10*), a result compatible with current measurements (*17*). Our dipolar supersolid does not move in a 1D configuration as in the Leggett model but has a more complex dynamics in the whole (x,y) plane, with both motion along the x axis, where the density modulation forms, and rotation of the individual droplets. Therefore, we expect Eq. 4 to account only for the superfluid fraction related to the dynamics along x, because it does not consider the superfluidity of the individual droplets.

Because we cannot measure $\rho(x)$ experimentally, we used numerical calculations (*30*). The right side of Eq. 4 is shown in Fig. 3 as triangles. It drops from unity for the BEC to ~0.3 for the supersolid, a relatively large value set by the large overlap between the two central droplets (Fig. 3, inset). It then decreases for increasing ε_{dd}, reaching almost zero at $\varepsilon_{dd} = 1.5$, where the droplets overlap almost vanishes. In that regime, one can recover the finite superfluid fraction of the numerical calculations by considering the droplets' superfluidity. Indeed, applying Eq. 2 to the case of independent droplets and considering that each droplet's moment of inertia about its axis is zero because of the cylindrical symmetry (*30*), one obtains the estimate $f_s^{drop} \approx (1 - \beta)/(1 - \beta^2)$. Using the theoretical distributions, we get $f_s^{drop} \approx 0.5$ for all the data points in the supersolid regime (black diamonds in Fig. 3). This estimate is quite close to the numerical data point for f_s at $\varepsilon_{dd} = 1.5$, and >2 SDs below the experimental data point at $\varepsilon_{dd} = 1.45$. Together with the qualitatively similar reduction of the two theoretical datasets for increasing ε_{dd}, this suggests that the mechanism identified by Leggett might have a relevant role in our small dipolar supersolid. To obtain a quantitative assessment, one will need further measurements and a theoretical analysis based on a 2D analog of the Leggett result (*36*, *37*).

We have established the superfluid nature of the dipolar supersolid by characterizing its nonclassical rotational inertia. The supersolid is different from standard superfluids because of the reduced superfluid fraction caused by the spontaneous breaking of translational invariance. The techniques that we have demonstrated, with an improvement of the measurement precision and of the resolution on ε_{dd}, will allow testing whether the superfluid fraction of the supersolid is indeed smaller than unity. Achieving larger systems might also allow studying the supersolid behavior in an annular geometry or in a 2D configuration, as well as studying the dynamics of quantized vortices in the supersolid phase (*29*).

REFERENCES AND NOTES

1. A. B. Migdal, *Sov. Phys. JETP* **10**, 176–185 (1960); http://www.jetp.ac.ru/cgi-bin/dn/e_010_01_0176.pdf.
2. G. B. Hess, W. M. Fairbank, *Phys. Rev. Lett.* **19**, 216–218 (1967).
3. P. J. Hakonen *et al*., *Phys. Rev. Lett.* **48**, 1838–1841 (1982).
4. F. Chevy, K. W. Madison, J. Dalibard, *Phys. Rev. Lett.* **85**, 2223–2227 (2000).
5. M. W. Zwierlein, J. R. Abo-Shaeer, A. Schirotzek, C. H. Schunck, W. Ketterle, *Nature* **435**, 1047–1051 (2005).
6. K. G. Lagoudakis *et al*., *Nat. Phys.* **4**, 706–710 (2008).
7. A. J. Leggett, in *Quantum Liquids: Bose Condensation and Cooper Pairing in Condensed-Matter Systems*, (Oxford Univ. Press, ed. 1, 2006), pp. 20–26.
8. A. F. Andreev, I. M. Lifshitz, *Sov. Phys. JETP* **29**, 1107–1113 (1969).
9. G. V. Chester, *Phys. Rev. A* **2**, 256–258 (1970).
10. A. J. Leggett, *Phys. Rev. Lett.* **25**, 1543–1546 (1970).
11. A. J. Leggett, *J. Stat. Phys.* **93**, 927–941 (1998).
12. M. H. W. Chan, R. B. Hallock, L. Reatto, *J. Low Temp. Phys.* **172**, 317–363 (2013).
13. E. Kim, M. H. W. Chan, *Nature* **427**, 225–227 (2004).
14. E. Kim, M. H. W. Chan, *Science* **305**, 1941–1944 (2004).
15. J. Day, J. Beamish, *Nature* **450**, 853–856 (2007).
16. D. Y. Kim, M. H. W. Chan, *Phys. Rev. Lett.* **109**, 155301 (2012).
17. A. Eyal, X. Mi, A. V. Talanov, J. D. Reppy, *Proc. Natl. Acad. Sci. U.S.A.* **113**, E3203–E3212 (2016).
18. J. Nyéki *et al*., *Nat. Phys.* **13**, 455–459 (2017).
19. L. Tanzi *et al*., *Phys. Rev. Lett.* **122**, 130405 (2019).
20. F. Böttcher *et al*., *Phys. Rev. X* **9**, 011051 (2019).
21. L. Chomaz *et al*., *Phys. Rev. X* **9**, 021012 (2019).
22. L. Tanzi *et al*., *Nature* **574**, 382–385 (2019).
23. M. Guo *et al*., *Nature* **574**, 386–389 (2019).
24. G. Natale *et al*., *Phys. Rev. Lett.* **123**, 050402 (2019).
25. N. L. Iudice, F. Palumbo, *Phys. Rev. Lett.* **41**, 1532–1534 (1978).
26. D. Guéry-Odelin, S. Stringari, *Phys. Rev. Lett.* **83**, 4452–4455 (1999).
27. F. Zambelli, S. Stringari, *Phys. Rev. A* **63**, 033602 (2001).
28. O. M. Maragò *et al*., *Phys. Rev. Lett.* **84**, 2056–2059 (2000).
29. S. M. Roccuzzo, A. Gallemí, A. Recati, S. Stringari, *Phys. Rev. Lett.* **124**, 045702 (2020).
30. Materials and methods are available as supplementary materials.
31. Y. Pomeau, S. Rica, *Phys. Rev. Lett.* **72**, 2426–2429 (1994).
32. R. M. W. van Bijnen, N. G. Parker, S. J. J. M. F. Kokkelmans, A. M. Martin, D. H. J. O'Dell, *Phys. Rev. A* **82**, 033612 (2010).
33. I. Ferrier-Barbut *et al*., *Phys. Rev. Lett.* **120**, 160402 (2018).
34. A. L. Fetter, *J. Low Temp. Phys.* **16**, 533–555 (1974).
35. A. S. C. Rittner, J. D. Reppy, *Phys. Rev. Lett.* **97**, 165301 (2006).
36. C. Josserand, Y. Pomeau, S. Rica, *Phys. Rev. Lett.* **98**, 195301 (2007).
37. A. Aftalion, X. Blanc, R. L. Jerrard, *Phys. Rev. Lett.* **99**, 135301 (2007).
38. L. Tanzi *et al*., Data for: Evidence of superfluidity in a dipolar supersolid from nonclassical rotational inertia. Zenodo (2020); https://doi.org/10.5281/zenodo.4288848.

ACKNOWLEDGMENTS

We thank E. Lucioni for contributions to the early stages of the experiment; A. Gallemi, A. Recati, S. Roccuzzo, and S. Stringari for discussions and for providing the theoretical data; D. E. Galli for discussions; and A. Barbini, F. Pardini, M. Tagliaferri, and M. Voliani for technical assistance. **Funding:** This work was supported by the EC-H2020 research and innovation program (grant no. 641122 - QUIC). **Author contributions:** L.T., A.F., C.G., and G.M. developed the experimental methods. L.T., J.G.M., G.B., and C.G. acquired the experimental data. L.T., J.G.M., G.B., C.G., and G.M. analyzed the data. G.B. performed the comparison with Leggett's theory. All authors contributed to the discussion and to manuscript preparation. **Competing interests:** The authors declare no competing interests. **Data and materials availability:** All data needed to evaluate the conclusions in the paper are present in the main text or the supplementary materials. All data have been uploaded to Zenodo (*38*).

SUPPLEMENTARY MATERIALS

science.sciencemag.org/content/371/6534/1162/suppl/DC1
Materials and Methods
Fig. S1
Table S1
References (*39*–*47*)

4 December 2019; accepted 2 February 2021
Published online 18 February 2021
10.1126/science.aba4309

Science

Evidence of superfluidity in a dipolar supersolid from nonclassical rotational inertia

L. TanziJ. G. MalobertiG. BiagioniA. FiorettiC. GabbaniniG. Modugno

Science, 371 (6534), • DOI: 10.1126/science.aba4309

A supersolid rotation

When a bucket of water is rotated, the water rotates with the vessel, contributing to the total moment of inertia. If such an experiment were done with a superfluid, it would decouple from the vessel and would not contribute to rotation. Tanzi *et al.* studied an intermediate case, a supersolid, which is predicted to only partially decouple, resulting in a moment of inertia smaller than the classical value. Whereas previous such experiments were done with helium, the authors used a gas of highly magnetic dysprosium atoms in an optical trapping potential that was suddenly changed, causing the gas to oscillate. Measuring the frequency of these oscillations provides evidence for a reduced moment of inertia.

Science, this issue p. 1162

Science (ISSN 1095-9203) is published by the American Association for the Advancement of Science. 1200 New York Avenue NW, Washington, DC 20005. The title *Science* is a registered trademark of AAAS.